EEET ECOLOGICAL ENGINEERING & ENVIRONMENTAL TECHNOLOGY

Ecological Engineering & Environmental Technology 2024, 25(9), 37–53
https://doi.org/10.12912/27197050/190084
ISSN 2299–8993, License CC-BY 4.0

Received: 2024.06.01
Accepted: 2024.07.10
Published: 2024.08.01

Optimization of *Olea europaea* Stone-Activated Carbon Preparation Using Response Surface Methodology for Thiamphenicol Removal in a Fixed Bed Column

Nora Samghouli[1], Imane Bencheikh[1], Karima Azoulay[1], Souad El Hajjaji[1*], Najoua Labjar[2]

[1] LS3MN2E-CERNE2D, Faculty of Sciences, Mohammed V University in Rabat, Av Ibn Battouta, B.P. 1014, Rabat 10000, Morocco

[2] LS3MN2E-CERNE2D, ENSAM, Mohammed V University in Rabat, Av Ibn Battouta, B.P. 1014, Rabat 10000, Morocco

* Corresponding author's e-mail: souad.elhajjaji@fsr.um5.ac.ma

ABSTRACT

The study addresses the persistent issue of thiamphenicol (THI) accumulation in aquatic environments and its detrimental impact on biological systems. While activated carbon is commonly used for removing such organic micropollutants in advanced wastewater treatment, this research explores the innovative use of olive stones as a feedstock for activated carbon production. The novelty of this study lies in the optimization of the activated carbon preparation process using a fractional factorial design with five critical factors: concentration, heating rate, activation temperature, activation time, and impregnation ratio. By employing the methylene blue method to determine the specific surface area (SSA), the optimal conditions were identified: a phosphoric acid solid-liquid ratio of 1:2 (74.52%), a heating temperature of 550 °C at a rate of 10 °C/min, and an activation period of 120 minutes, resulting in an SSA of 53.07 m^2/g. The subsequent THI adsorption tests in a fixed-bed column revealed that THI removal efficiency was inversely proportional to flow rate and initial THI concentration, while positively correlated with bed height. This study fills a critical gap by demonstrating an effective, sustainable method for producing activated carbon from agricultural waste, optimizing the process parameters for maximum efficiency in micropollutant removal.

Keywords: olive fruit stones, activated carbon, response surface methodology, thiamphenicol, adsorption, fixed bed column.

INTRODUCTION

Even small amounts of emerging contaminants, known as micropollutants, pose major hazards to aquatic ecology. Hospital, household, and industrial activities generate them, either directly or indirectly (Mailler et al., 2017). Pharmaceutical micropollutants are the most widespread and dangerous pollutants for aquatic biota; therefore, they are considered a main emerging issue (Busch et al., 2016). Recently, a great deal of interest has been focused on the use of veterinary antibiotics (VAs), which are considered hazardous to the environment, in veterinary and human medicine. Between 17% and 90% of VAs are eliminated as the active component after being administered to animals, and they subsequently enter the environment via their faeces or urine (Carvalho and Santos, 2016). Thiamphenicol (THI) is a common antibiotic used to control bacterial illnesses and is used in aquaculture and animal husbandry (Li et al., 2014). However, the negative effects of THI, such as its hematotoxicity, embryotoxicity, and potent immunosuppressive activity, affect how well plant microbes function physiologically and in animals (Maita et al., 1999). THI may also enter surface wastewater and water through animal metabolism, wastewater discharge, and rain runoff, which readily produces toxins in humans and the environment via the food chain (Sim et al.,

2011). Thus, a practical and highly effective technique is required to eliminate THI from water.

To eliminate organic contaminants from wastewater and water, activated carbon (AC) has been employed extensively (Sabio et al., 2006; Sotelo et al., 2014, 2012a). AC has several advantages, and its main features are its large surface area and simple regeneration by solar energy (Miguet et al., 2016; Suhas et al., 2016). AC has a highercapacity of absorption and can be useful in the removal of some organic pollutants. According to certain research, AC has a 100% removal efficiency. Adsorption by AC is used in column mode in practical operations (Putra et al., 2009). In terms of cost ratio and quality, chemical activation offers the best end product and has been more thoroughly investigated in previous research than physical activation (Heidarinejad et al., 2020a). An activating agent is often either a basic or an acid. Potassium hydroxide and phosphoric acid are the most effective activating agents (Azmi et al., 2015; Balogoun et al., 2015; Gueye et al., 2014; Heidarinejad et al., 2020b; Li et al., 2017). The primary factors influencing the quality of AC are the impregnation ratio, time and temperature of activation, concentration, and heating rate (Das and Mishra, 2017). These major variables could be optimised using the RSM method for preparing the AC solution (Asfaram et al., 2015; Senthilkumar et al., 2017). Research in the literature indicates that AC possesses both a high removal effectiveness and a high adsorption capacity. The removal efficiency in some applications can reach 100%. Furthermore, the USEPA Agency has recognized AC as a better technique for treating a variety of controlled organic pollutants (Sotelo et al., 2012b). The column mode is used in a number of applications and experimental studies for AC adsorption treatment (Patel et al., 2022). Column adsorption offers several benefits, including a straightforward mode of operation, effective process control, and the potential for high removal efficiencies. Moreover, the procedure may be easily expanded from the laboratory to industrial implementation.

Various biomasses, such as coconut tree waste (Freitas et al., 2019; Jawad et al., 2017), peach stones, rice husk (Álvarez-Torrellas et al., 2016), bagasse from sugarcane (Chakraborty et al., 2018), palm shell (Mustafa et al., 2022) and raw bamboo (Ismail et al., 2022), have been used for AC preparation. In this study, olive fruit stones were chosen because of their abundance in the Mediterranean region. Olive stones are well known and abundant agricultural byproducts in regions where they are widely farmed. Approximately 57% of Morocco's total tree acreage is made up of olive trees, which are the primary fruit species cultivated there (Elabdouni et al., 2020). This variety of fruit may be found all across the country since it can adapt to any bioclimatic zone in Morocco. Many studies have been conducted on the AC efficiency of common contaminants obtained from olive stone waste, including dyes (Al-Ghouti and Sweleh, 2019; Hazzaa and Hussein, 2015) as well as heavy metals (Alslaibi et al., 2013; Corral-Bobadilla et al., 2021). The adsorption of emerging pollutants, such as ketoprofen, has been studiednaproxen, diclofenac (Baccar et al., 2012), amoxicillin (Mansouri et al., 2015), and ibuprofen (Mansouri et al., 2015), using olive stone AC; the related adsorbed quantities were respectively 24.7, 39.5, 56.2, 158.83 and 178.04 $mg.g^{-1}$. In this study, we investigated the adsorption capabilities of carbon derived from olive fruit stones, chemically activated with H_3PO_4, for removing THI. Our research focused on utilizing this innovative adsorbent, derived from agricultural waste, for effective THI removal.

MATERIALS AND METHODS

Preparation of feedstock

Olive fruit stones (*Olea europaea*) from the Errachidia province of Morocco were used as precursor material. This material was collected, previously washed in water, and then dried. The following step consists of crushing the olive stones into smaller fragments by mechanical grinding. Then, we sieved them to obtain particles with sizes between 400 μm < G < 640 μm. The grains were repeatedly rinsed with hot distilled water until aroma disappeared and rinse water was clear. They were then oven-dried for 24 hrs at 110 °C.

Activated carbon preparation of and statistical experimental design approach

Approximately 20 g of sample was inserted into a covered crucible and then heated at 400 °C by a muffle furnacefor an hour with 5 °C per minute as rate in an anoxic environment. This was how the carbonization procedure was carried out. After cooling, the samples were cooled to room temperature. In this work, a statistical

experimental design was used with JMP[11] software to define variables for activation. To optimize these processes, the surface of RSM, a statistical and mathematical set of techniques, is adequate. The goal is to maximize the reaction, which is affected by a number of variables (Baş and Boyacı, 2007). The RSM model is a whole quadratic Equation 1 or a shortened version of it. The following equation represents the second-order model:

$$Y = \beta_0 + \sum_{j=1}^{k} \beta_j X_j + \sum_{j=1}^{k} \beta_{jj} X^2_j + \sum \sum_{i<j} \beta_{ij} X_i X_j \quad (1)$$

In this Equation, Y represents the anticipated response, β_0 denotes the coefficient intercept, βi, β_{ii}, β_{ij} signifies respectively the linear, the squared and interaction terms, as well as X_i and X_j are coded as independent variables.

With the fewest number of tests, the CCD design and RSM model may be used to adjust the surface to maximize the important factors and explore the relationships and interplay between the parameters (Hameed et al., 2008).

The AC by phosphoric acid (ACPA) depends on several parameters. To determine the ideal efficiency settings for each variable that guarantees a high specific surface area (SSA "Y") computed using the methylene blue technique. The methylene blue (MB) value is considered to have the greatest response when AC is being prepared (Itodo et al., 2010).The MB approach was employed to determine the surface area that was accessible to relatively large molecules in the sample. Twenty-five millilitres of the solution of methylene blue was taken at various concentrations, and 0.1 g of the sample was mixed for two hours before being centrifuged and tested. Equation 2 can be applied to calculate the surface area using Langmuir's isotherm (Azoulay et al., 2020).

$$SSA = \frac{b \times N \times S}{M} \quad (2)$$

where: SSA is the surface area (m^2g^{-1}); b is the maximal capacity of adsorption (mg/g) obtained from the isotherm of Langmuir; N stand to the Avogadro number, M hydrated MB molar mass (319.86 g/mol); and S is the surface area covered by methylene blue molecules (119 Å²). A two-level and five-factor central composite design (CCD) (weight % of phosphoric acid (wt% PhA), solid–liquid ratio, temperature, heating rate, and activation time) was used in our study as the experimental design (Baccar et al., 2012; García-Mateos et al., 2015; Mansouri et al., 2015; Sun et al., 2012).

These important parameters will have an impact on the resulting AC properties. Table 1 indicate the independent variables' as well as their coded levels. To facilitate the regression, the variables' values were coded, with + 1 denoting the highest level and -1 denoting the lowest level.

The fractional factorial design experiment 2^{k-r} was completed by a start design experiment 2 × k and replicated center experimental point N_0 (the number of center points in this study is 3) with K = the number of variables; in our study, we have five variables and r = the fraction of the full factorial, which is equal to 1. Thus, the required experiments number (N) is determined by $N = 2^{k-r} + 2k + N_0$ (Bencheikh et al., 2021; Bhattacharya, 2021; Tarley et al., 2009).

The output data were statistically evaluated using variance analysis (ANOVA). In addition, we aimed to determine the best conditions for carbon activation as well as the significance and impact of factors both independent and interacting in the modelling.

Characterization of the optimized activated carbon by phosphoric acid (OACPA)

Many methods have been adopted to analyse AC samples, in particular XRD, FTIR and N_2 adsorption–desorption isotherm analysis (Quantachrome Touchwin™ v1. 22). These techniques are required to provide information on the characteristics of such synthesized AC, which is helpful for further understanding.

Spectral characterization: Using a KBr disc and a burka-tensor 27 spectrometer in reflection mode, the FT-IR spectrum of the optimal AC was recorded between 400 cm^{-1} and 4000 cm^{-1}.

X-ray powder diffraction (XRD) analysis was employed to investigate the phase/crystallographic composition of the optimum AC.

Adsorbate preparation

Adsorption was carried out on thiamphenicol's active ingredient (97.5% purity. Each chemical used in this study is of the analytical class. A stock solution of 100 $mg \cdot L^{-1}$ was obtained by dissolving thiamphenicol (100 mg) in 1 liter of distilled water in a 1 liter measuring flask.The THI of the solution was detectable at a wavelength of

Table 1. Variables with coded levels according to the central composite design

Parameter		Levels				
Variables	Symbols	-α	-1	0	+1	+α
Phosphoric acid weight %	X_1	29.52	40	57.26	85	85
Activation time (min)	X_2	41.78	60	90	120	138.22
Solid–Liquid (ratio)	X_3	0.17	0.25	0.38	0.5	0.58
Heating rate (°C.min^{-1})	X_4	8.48	10	12.5	15	16.52
Temperature (°C)	X_5	419.64	450	500	550	580.36

225 nm, and all studied solutions were measured with a Shimadzu UV-1900i spectrophotometer.

Studies in stationary bed columns

Experimental process

The use of mini-columns in the study of adsorption dynamics constitutes a simple method (Rosene et al., 1976). In this work, the adsorbent was placed in a column (1.4 cm in diameter), where process of adsorption took place. The rate of the adsorbate passes into the column. To guarantee that the materials inside the column were secure, a layer of support cotton was placed on the bottom of the column. First, cotton was placed for prevention the adsorbent from sliding off the column; the necessary amount of AC was then added to the column. The second layer of cotton was positioned on top of the adsorbent bed to guarantee that the adsorbent within the column was unable to move. The effects of bed height, starting THI concentration, and THI flow rate were the three main factors of this investigation. A peristaltic pump managed the volume of fluid in the fixed-bed column at any given time. The desired sample solution was continuously collected at the exit as the solution flowed into the column. A UV spectrophotometer was employed to measure the treated water concentration. All findings from this study, carried out at a pH of 5.7 and in 24 °C, were used to analyse the breakthrough curve.

Flow rate effect

The effects of various rates (1 mL/min and 4 mL/min) on THI adsorption by the optimal AC of phosphoric acid were investigated. The concentration of THI as well as adsorbent bed height were initially maintained at 15 mg·L^{-1} and 1 cm.

Initial THI concentration effect

Initial concentrations of THI (5.5 mg·L^{-1}, 15 mg·L^{-1}) were investigated for their effect on the adsorption efficacy of optimal AC by phosphoric acidwith a height of 1cm and 1 ml.min^{-1}as rate.

Bed-depth effect

The optimal AC effect of phosphoric acid on the THI was examined at 1 cm, 1.7 cmofbed-heights. THI was added at a fixed starting concentration (15 mg·L^{-1}) with 1 mL·min^{-1} asrate.

Adsorption column performance

The performance and reactivity of a column are highly influenced by the onset time and the breakthrough curve form. Operating properties, in particular the throughput rate, initial adsorbate concentration and bed height, have a significant impact on the experimental determination of these parameters. The breakthrough curve, which is typically represented by C_t/C_0 versus time (Delgado et al., 2022), illustrates how a drug is loaded into a fixed bed to be removed from the solution. Equations 3, 4, 5 and 6 of the effluent volume (V_{eff}), the total quantity of adsorbate adsorbed (q_{total}), the amount applied to the column (m_{total}), and the total adsorbate removal percentage (%R) (Cruz-Olivares et al., 2013; Kavianinia et al., 2012) are calculated as follows:

$$V_{eff} = Qt_{total} \tag{3}$$

$$q_{total} = \frac{Q}{1000}\int_{t=0}^{t=t} Cads\ dt \tag{4}$$

$$m_{total} = \frac{QC_0t_{total}}{1000} \tag{5}$$

$$\%R = \frac{q_{total}}{m_{total}} \times 100 \tag{6}$$

where: t_{total} represents the overall duration of fluid flow through the column (in minutes); Q stands for the solution volume at a particular instant (in mL/min); q_{total} is the total adsorbate adsorbed in mg/g, where the adsorbed pollutant concentration is calculated by $Cads = (C_0 - C_e)$; C_e (mg/g) as well as C_0 (mg.L^{-1}) are the effluent and influent

pollutant concentrations; and m_{total} is the total adsorbate applied to the column in mg.

RESULTS AND DISCUSSION

Experimental design for optimizing activated carbon preparation

The experimental design was applied using JMP[11] software, and central composite design (CCD) was used to correlate the specific surface area (SSA (m^2/g)) calculated by the methylene blue value (Y) with the phosphoric acid weight % (X_1), solid – liquid ratio (X_2), temperature (X_3), heating rate (X_4), and activation time (X_5). The most important feature of AC in the adsorption process is its specific surface area. The number of experiments required N = 25 - 1 + 2 × 5 + 3 = 29 is the total number of tests required for the experiments required for statistical modelling. The experimental design data set and the response values noted in the experimental outcomes are shown in Table 2.

Variance analysis

Analysis of variance is a crucial statistical technique for evaluating the validity of a model.

Table 2. Experimental design results of the ACs studied

Run	Coded level					Actual parameters					Response
						X_1	X_2	X_3	X_4	X_5	Y
	X_1	X_2	X_3	X_4	X_5	Phosphoric acid weight %	Activation time (min)	Solid–Liquid (ratio)	Heating rate (°C/min)	Temperature (°C)	SSA (m^2/g)
1	-1.61	0	0	0	0	29.52	90	0.375	12.5	500	0.92
2	-1	-1	-1	-1	-1	40	60	0.25	10	450	9.09
3	-1	-1	-1	1	1	40	60	0.25	15	550	5.97
4	-1	-1	1	-1	1	40	60	0.5	10	550	9.10
5	-1	-1	1	1	-1	40	60	0.5	15	450	6.86
6	-1	1	-1	-1	1	40	120	0.25	10	550	6.79
7	-1	1	-1	1	-1	40	120	0.25	15	450	9.86
8	-1	1	1	-1	-1	40	120	0.5	10	450	4.94
9	-1	1	1	1	1	40	120	0.5	15	550	27.43
10	0	-1.61	0	0	0	57.26	41.78	0.38	12.5	500	7.30
11	0	0	-1.61	0	0	57.26	90	0.17	12.5	500	8.53
12	0	0	0	-1.61	0	57.26	90	0.38	8.48	500	11.29
13	0	0	0	0	-1.61	57.26	90	0.38	12.5	419.64	8.36
14	0	0	0	0	0	57.26	90	0.38	12.5	500	9.29
15	0	0	0	0	0	57.26	90	0.38	12.5	500	9.99
16	0	0	0	0	0	57.26	90	0.38	12.5	500	8.92
17	0	0	0	0	1.61	57.26	90	0.38	12.5	580.36	10.74
18	0	0	0	1.61	0	57.26	90	0.38	16.52	500	9.51
19	0	0	1.61	0	0	57.26	90	0.58	12.5	500	4.39
20	0	1.61	0	0	0	57.26	138.22	0.38	12.5	500	5.17
21	1	-1	-1	-1	1	74.52	60	0.25	10	550	19.63
22	1	-1	-1	1	-1	74.52	60	0.25	15	450	7.96
23	1	-1	1	-1	-1	74.52	60	0.5	10	450	8.49
24	1	-1	1	1	1	74.52	60	0.5	15	550	7.06
25	1	1	-1	-1	-1	74.52	120	0.25	10	450	0.99
26	1	1	-1	1	1	74.52	120	0.25	15	550	8.72
27	1	1	1	-1	1	74.52	120	0.5	10	550	57.23
28	1	1	1	1	-1	74.52	120	0.5	15	450	5.68
29	1.61	0	0	0	0	85	90	0.38	12.5	500	8.98

When the response variable is influenced by random variations, the model's variance is assessed using the regression mean square. For a robust model, the regression mean square and the ratio of the residual mean square should ideally converge to unity, indicating a good fit (Bouiti et al., 2024).

In this study, a 95% confidence level was set as the threshold for statistical significance. The primary aim was to determine whether the proposed model could accurately capture the inherent variability within the data. By examining both inter-group and intra-group variations, ANOVA provides the necessary analytical framework to achieve this objective.

In this research, an analysis of variance was carried out to establish the statistical significance of the proposed models (Samghouli et al., 2022) for the specific surface area (Y) and the independent variables (X_1, X_2, X_3, X_4, and X_5). The results acquired from the variance analysis of the specific surface area of the carbon activated by phosphoric acid are shown in the Table 3.

Table 3 presents the results of variance analysis for the response's coded modelling. The data show that the proposed model for the SSA of activated carbon by phosphoric acid (Y) is statistically significant at the 5% confidence level (p values $\leq$ 0.05) (Azoulay et al., 2020; dos Reis et al., 2016) and that SSA (p value = 0.04) has a p-value inferior to 0.05. The correlation coefficient of the AC specific surface area studied is 0.89 (Figure 1a), and the RSq_{Adj} is 0.64, which probably indicates the compatibility between the data and the model. The SSA of the AC residue from each experiment is shown in Fig. 1b. Therefore, the residue graph shows a reasonable spatial distribution, proving that the model adequately describes this study.

Estimated parameters and mathematical model

Analysis of the pvalues for the interplay between time and solid–liquidratio, the interplay between phosphoric acid weight and heating rate, the temperature, the interplay between time and temperature, and the interplay between solid/liquidratio and temperature showed that those variables were probably statistically significant for the specific surface area, with p values of 0.01, 0.01, 0.01, 0.02, and 0.04, respectively. The p-values of remaining factors were greater than 0.05, which indicates statistically insignificant. (Di Leo and Sardanelli, 2020; dos Reis et al., 2016).

Based on Table 4's results, the complexity of the regression analysis model was minimized by eliminating all no significant components, and the best fit of the second-order polynomial model equations is given by Equation 7. This equation describes the SSA of the AC by phosphoric acid, and the signs positive and negative before each

Table 3. Analysis of variance for the quadratic polynomial surface response modelling of carbon activation by phosphoric acid

Source	DF	Sum of squares	Mean square	F Ratio
Model	20	2655.77	132.79	3.49
Error	8	303.82	37.98	P value
Total corrected	28	2959.59		0.04*

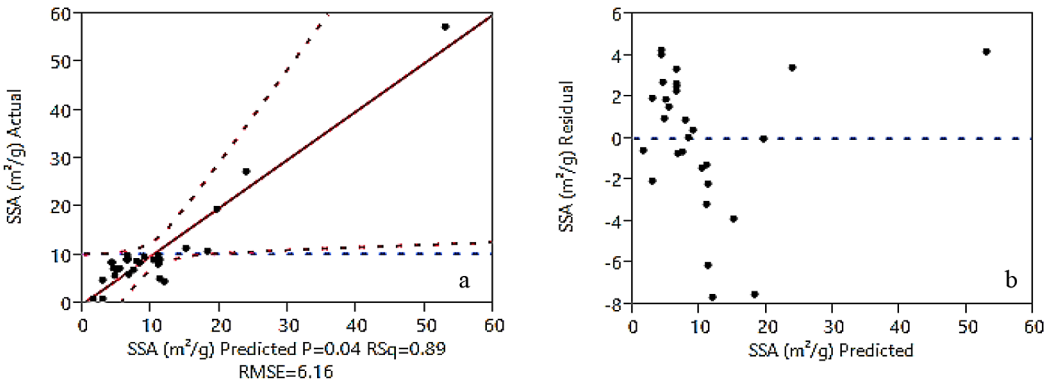

Figure 1. (a) Experimental predicted response and (b) analysis of the residual of the specific surface area SSA of AC

Table 4. Estimated effects for the model of the quadratic polynomial of SSA (*indicates that the correlation term is statistically significant)

Term	Estimate	Std Error	t Ratio	P value
Model	6.62	2.76	2.40	0.04*
X_1 (Wt%PhA)	2.30	1.34	1.72	0.12
X_2 (time)	2.08	1.34	1.55	0.15
X_3 (Solid–Liquid (ratio))	2.41	1.34	1.80	0.11
X_4 (Heating rate)	-1.86	1.34	-1.40	0.20
X_5 (Temperature)	4.34	1.34	3.24	0.01*
$X_1 \cdot X_2$ (Wt%PhA*time)	0.71	1.54	0.47	0.65
$X_1 \cdot X_3$ (Wt%PhA · Solid–Liquid (ratio))	1.53	1.54	1.00	0.35
$X_2 \cdot X_3$ (time · Solid–Liquid (ratio))	5.01	1.54	3.25	0.01*
$X_1 \cdot X_4$ (Wt%PhA · Heating rate)	-4.82	1.54	-3.13	0.01*
$X_2 \cdot X_4$ (time · Heating rate)	0.01	1.54	0.01	0.99
$X_3 \cdot X_4$ (Solid–Liquid (ratio) · Heating rate)	-1.80	1.54	-1.17	0.27
$X_1 \cdot X_5$ (Wt%PhA · Temperature)	3.19	1.54	2.07	0.07
$X_2 \cdot X_5$ (time (min) · Temperature)	4.34	1.54	2.81	0.02*
$X_3 \cdot X_5$ (Solid–Liquid (ratio) · Temperature)	3.85	1.54	2.50	0.03*
$X_4 \cdot X_5$ (Heating rate · Temperature)	-3.15	1.54	-2.04	0.07
$X_1 \cdot X_1$ (Wt%PhA · Wt%PhA)	0.02	1.66	0.01	0.99
$X_2 \cdot X_2$ (time · time)	0.52	1.66	0.31	0.76
$X_3 \cdot X_3$ (Solid–Liquid (ratio) · Solid–Liquid (ratio))	0.60	1.66	0.36	0.73
$X_4 \cdot X_4$ (Heating rate · Heating rate)	2.13	1.66	1.28	0.23
$X_5 \cdot X_5$ (Temperature · Temperature)	1.79	1.66	1.08	0.31

factor's coefficient correspond to the synergic and antagonistic effects, respectively.

$$Y = 6.62 + 5.01X_2X_3 - 4.82X_1X_4 + 4.34X_5 + 4.34X_2X_5 + 3.85X_3X_5 \quad (7)$$

Parameter optimization of the OACPA

The statistical approach helps in predicting the specific surface area max potential at the optimum level of the variables that are independent. We will determine the optimum conditions for maximum yield while minimising variability. According to Fig. 2, the maximum SSA of AC that may be achieved under optimal conditions is 65.27 m^2/g. The optimal conditions for obtaining the highest SSA of OACPA are reported in Table 5.

The 3D response surface plot (Fig 3.b) demonstrates that the effect of two independent factors (significant variables obtained in the model equation) on the specific surface area changes simultaneously. The AC of phosphoric acid (Fig. 3.b1) shows inter actions between the ratio of solid to liquid and the activation temperature, and the maximum specific surface area values correspond to the highest temperatures and biochar-H_3PO_4ratio. For the interplay between the solid–liquid ratio and time, the best specific surface area results were obtained with a longer activation time and a greater ratio of biochar-H_3PO_4 (Fig. 3. b2). Figure 3. b3 indicates the interplay between the activation temperature and time; the specific surface increases as both factors increase. On the other hand, the interplay between the phosphoric acid weight % and the heating rate showed that the SSA increased when the phosphoric acid weight % increased and the heating rate decreased (Fig 3. b4).

Table 5. Optimal conditions for obtaining a high specific surface area for RSM and validating the experimental results

Setting	Wt% PhA	Time (min)	Solid–liquid (ratio)	Heating rate (°C/min)	Temperature (°C)	SSA (m^2/g)	SSA (m^2/g) Lower	SSA (m^2/g) Upper	Desirability
Optimal condition	74.52	120	0.5	10	550	53.07	39.46	66.69	0.53

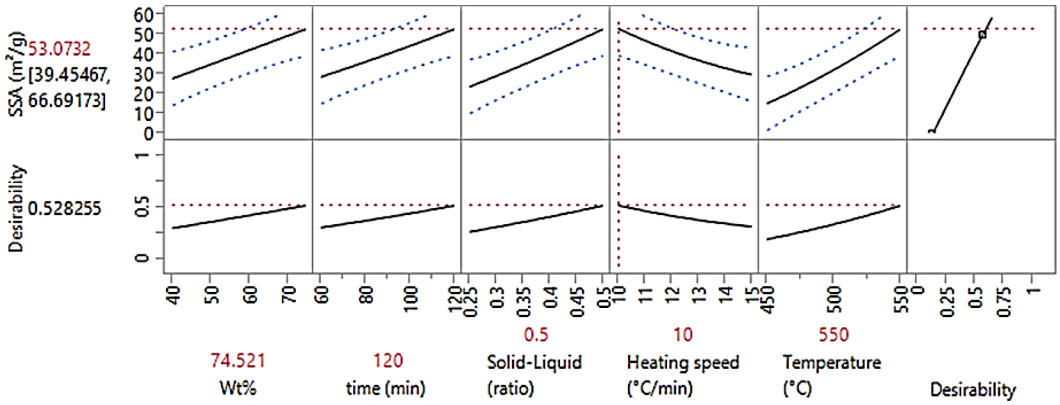

Figure 2. Prediction profiler showcasing the models and settings that contributes to achieving maximum overall desirability

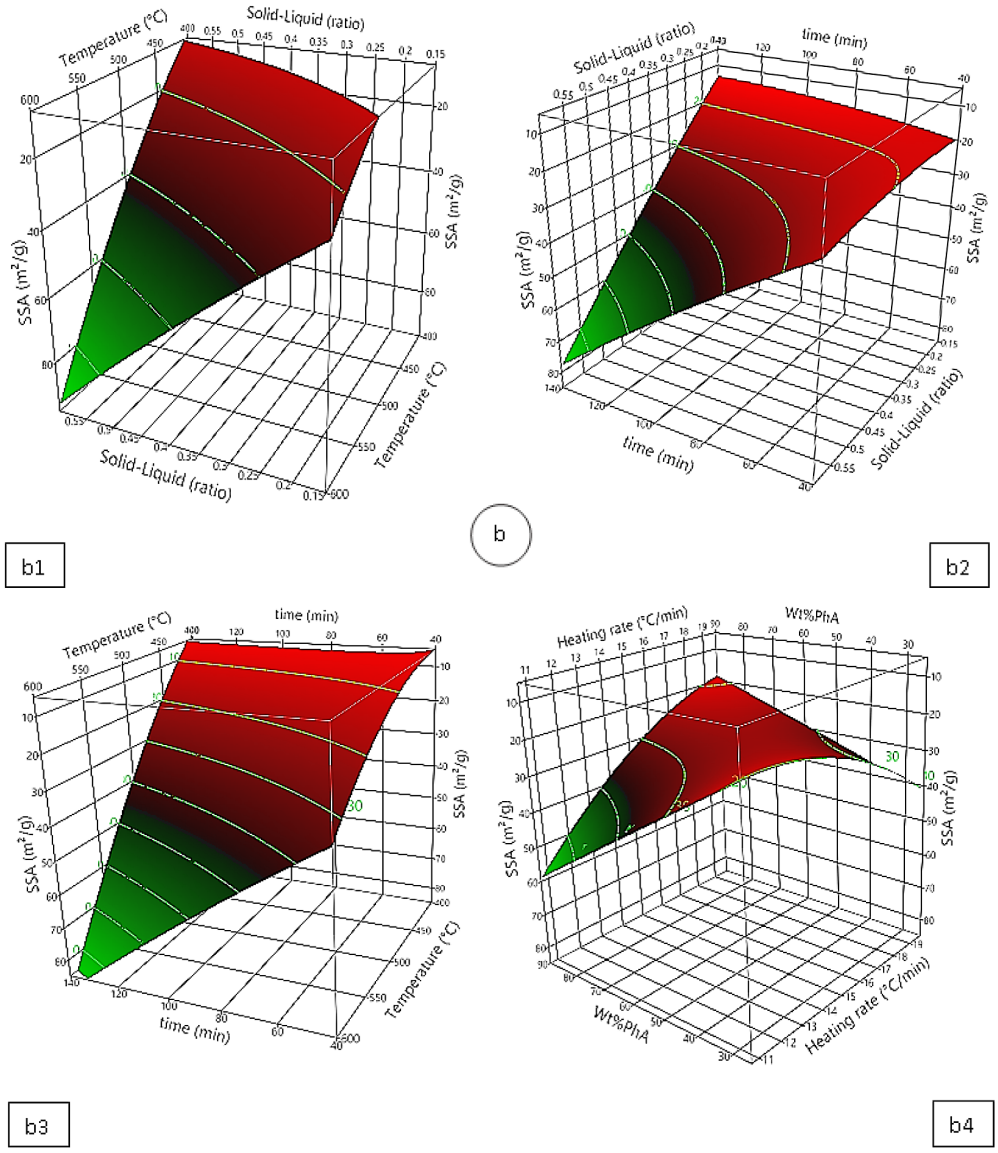

Figure 3. (b) Effect of independent variables in the three-dimensional response surface on the external surface area, (b1) effect of solid – liquidratio (0.25; 0.5) and temperature (450 °C; 550 °C), (b2) effect of time (60 min; 120 min) and solid–liquidratio (0.25; 0.5), (b3) effect of temperature (450 °C; 550 °C) and time (60 min; 120 min) and (b4) heating rate effect (10 °C.min^{-1};15 °C.min^{-1}) as well as Wt% of phosphoric acid (40%; 85%)

Characterization of OACPA

X-ray diffraction analysis

The diffractogram (Fig. 4) of the raw olive fruit stones shows that, in general, their structure is amorphous, and the peak at 2Θ = 22.5 corresponds to the cellulose structure (Kaya et al., 2018; Seydibeyoğlu et al., 2017).

The peak at approximately 2θ = 22° - 25° of OACPA was indexed as C (002) diffraction, revealing the amorphous structure of carbon with randomly oriented aromatic rings. The peak present at 2θ = 42°- 45° is related to the structure of C (100) graphite (Dehkhoda et al., 2014; Hu et al., 2014; Jamil et al., 2020).

FTIR analysis

The main peaks that appear in the spectrum of the raw olive fruit stone (Fig. 5) are attributed to lignin, cellulose, and hemicelluloses in the lignocelluloses' compounds. This result is similar to that obtained for the lignocelluloses' groups in other studies (Baccar et al., 2009). The band placed at 3304.23 cm^{-1} correspond to the vibrations O-H in the hydroxyl, phenol, as well as acid grps (Xu et al., 2013). Moreover, the high peaks at 2922 cm^{-1} as well as 2856 cm^{-1} are ascribed to C-H vibration stretching in alkyl groups. According to Xu et al. (Xu et al., 2013), these distinctive peaks represent lignin and hemicelluloses, respectively. At 1748 cm^{-1}, the carbonyl group C = O peak may be observed (Roğlu et al., 2017). The alkene group (C = C) vibrations are visible at approximately 1641.11 cm^{-1}, but the aromatic ring C = C vibrations are visible at approximately 1506.92 cm^{-1}. Alkyl and hydroxyl groups, which are the basic building blocks of lignocelluloses' groups, are responsible for the peaks at 1466 cm^{-1}as well as 1386 cm^{-1} (Baccar et al., 2009). The band at 1316 cm^{-1} could be corresponded to the vibrations C–O of carboxylate grps. The peak at 1254 cm^{-1} can be the result of phenol groups, ethers, or esters (Durán-Valle et al., 2005). The peaks corresponding to C-O stretching are located between 1160–1042 cm^{-1} (Baccar et al., 2009).

The FTIR spectrum of OACPA shows a few peaks that are comparable to those of raw olive fruit stones, verifying that the effect of phosphoric acid treatment was caused by significant chemical modifications. Considering the OACPA spectrum, the peak at 1039 cm^{-1} for OACPA decreased in intensity compared with that of the spectrum of the raw olive fruit stones. According to Jiang et al. (Jiang et al., 2012), this peak is assigned to P-O, indicating the reaction of H_3PO_4 with OACPA. It is hypothesized that phosphoric acid added oxygenated functional groups to the biochar, which is predicted to have significant effects on the performance of OACPA as an adsorbent. One possible explanation for the broad peak at 1163 cm^{-1} is the asymmetric stretching of O–P–O (Jiang et al., 2012). According to Benaddi et al., dehydrating cellulose using H_3PO_4 acid similarly to dehydrating

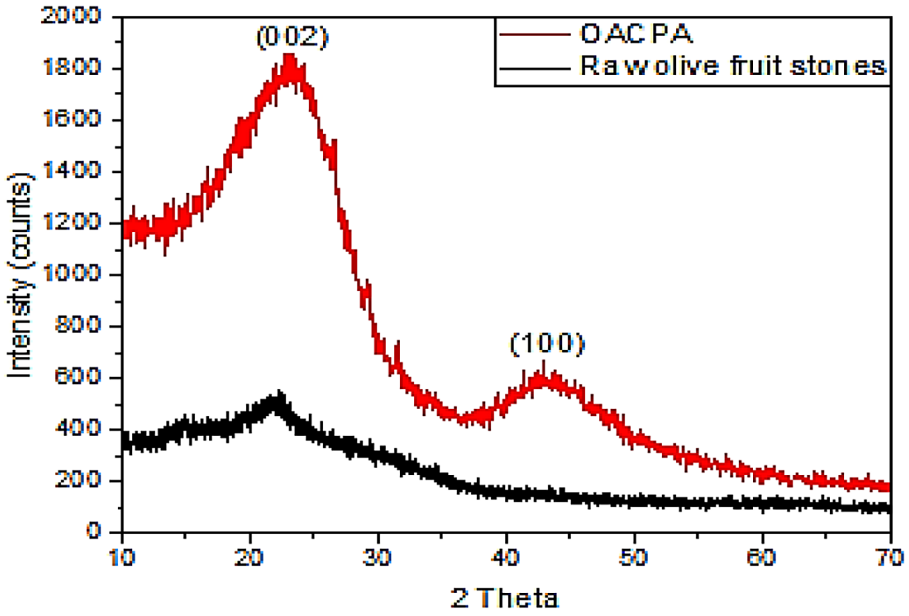

Figure 4. XRD patterns of the raw olive fruit stones and OACPA

alcohols. Moreover, they proposed that phosphorous oxides exhibit Lewis acid behaviour and could form the bonds C–O–P at elevated temperatures (Benaddi et al., 1998). The absence of peaks between 1254–1506.92 cm^{-1} was noted, except for the peak at 1316 cm^{-1}, which exhibited a reduction in intensity. Similar findings were reported in Benzekri et al., who suggested that this particular peak may arise from the asymmetric bending vibration of the $–CH_3$ group (Benzekri et al., 2018). The band at 1567.8 cm^{-1} corresponds to C = C in aromatic groups. This indicates that the amount of aromatic groups present in the structure of OACPA increased. A peak at 1641.11 cm^{-1} corresponding to alkene groups completely disappeared. A sharp reduction in the band intensity at 1748 cm^{-1} represents C = O groups. This implies that there are fewer C = O groups in OACPA than in the raw olive fruit stones. The impact of H_3PO_4 may be responsible for the decomposition of carbonyl groups and, subsequently, the decrease in the quantity of carbonyl groups. The disappearance of the peaks at 2922 cm^{-1}as well as 2856 cm^{-1}, which attributed to alkyl groups, and a clear decrease in the peak at 3304.23 cm^{-1} are observed; these results are similar to those of Song et al. (Song et al., 2011).

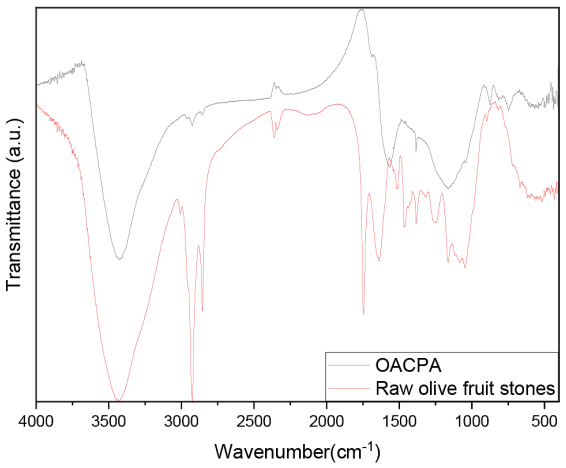

Figure 5. FTIR spectrum of raw olive stones as well as OACPA

Adsorption/desorption isotherms

The N_2 isotherms of OACPA and OFs are shown in Fig. 6. The SSA and total pore volume of the samples are given in the Table 6. The surface areas of the raw olive fruit stones and OACPA were 2.83 and 178.73 m^2/g, respectively. The surface area of OACPA was 63 times greater than that of the raw olive fruit stones. The total pore volumes of the raw olive fruit stones and OACPA were 0.0016 and 0.1035 $cm^3 \cdot g^{-1}$.

Adsorption column performance

Flow rate effect

The impact of the solution flow rates (1 mL/min and 4 mL/min) on the adsorption of THI by OACPA was investigated. The THI concentration and bed height of the adsorbent respectively were held constant (1 cm and 15 mg/L). The curves shown for the adsorbate flow rates in the column under study are displayed in Fig. 7. At the lowest rate (1 mL/min), the slowest progression curve, which shows how long it took to reach equilibrium, was produced. The low THI solution flow rate allowed the molecules of adsorbate more time for diffusion, increasing the quantity of THI adsorbed throughout the column. The saturation time required to accomplish

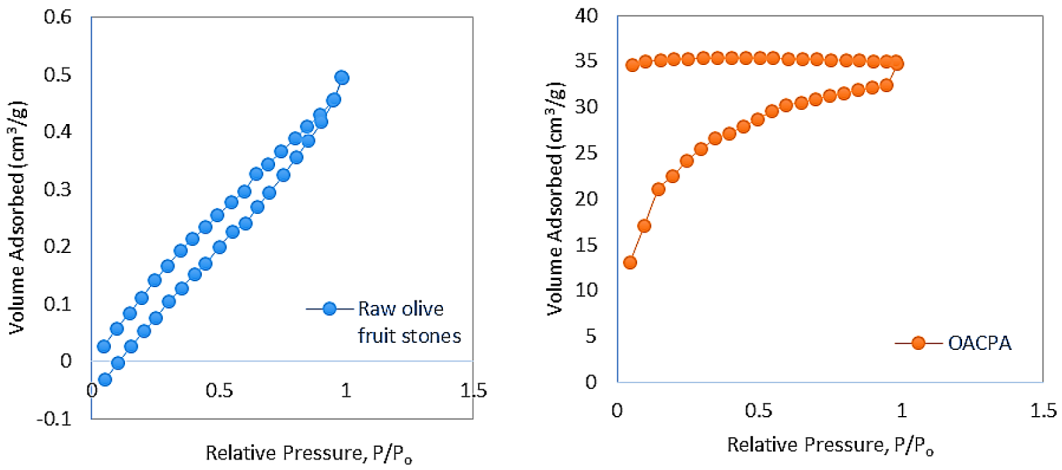

Figure 6. N_2 isotherms of raw olive fruit stones and OAPAC

Table 6. BET results of the samples

Samples	SSA (m^2/g)	Total pore volume (cm^3/g)
Olive fruit stones	2.83	0.0016
OACPA	178.73	0.1035

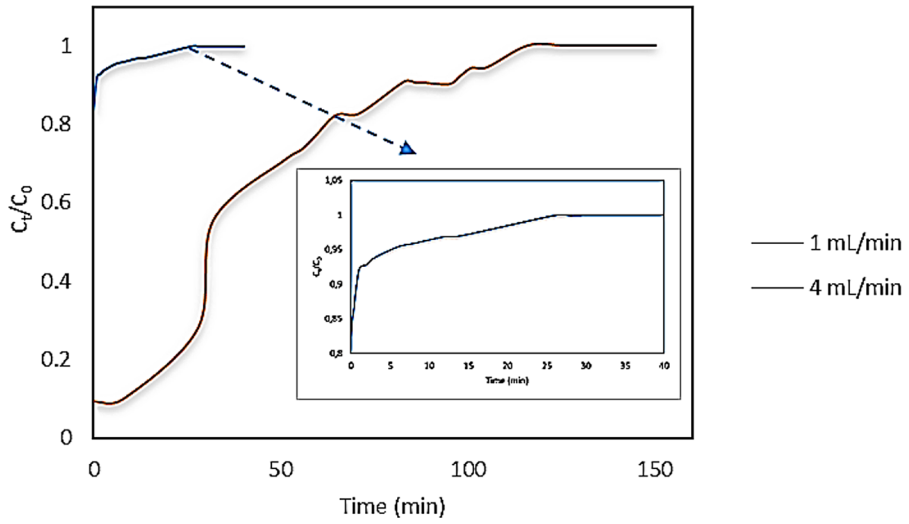

Figure 7. Breakthrough curves at different flow rates

breakthroughs drastically decreased at a THI rate of 4 mL·min^{-1}. The total volume increases with increasing flow rate, as shown in Table 7. The total absorbance (q_{total}) of AC at 1 and 4 mL/min was low at 0.41 and 0.036 mg, respectively, although that of the bed was not high. This resulted from the quick contact between THI and the adsorbent, which was caused by the fast adsorbate flow rate across the column. Due to the shorter adsorbent residence time in the column and as previously mentioned, the THI decreased from 23.56% to 2% as the THI flow rate increased from 1 to 4 mL/minute.

Bed high effect

Figure 8 displays the breakthrough curve plots for THI uptake to study the effect of bed height (1 cm and 1.7 cm). A THI (15 mg·L^{-1}), a flow rate (1 mL·min^{-1}), and bed heights (1 cm and 1.7 cm) were maintained as the operational parameters. The findings indicated a potential decrease in the breakthrough curve as the bed-height improved. The parameters for the breakthrough curve at varying bed heights are presented in Table 8. Furthermore, the breakthrough curves exhibited a decline with higher adsorbent concentrations in the bed, consequently extending the overall adsorption period from 116 to 140 minutes. This alteration occurred during the adsorption process because there were more active sites available on the adsorbent surface (Iheanacho et al., 2021).

Given that more adsorbent was present, a greater amount of bed took longer to reach saturation (Fallah and Taghizadeh, 2020). In addition, compared to when a shorter bed height was employed, an increase in the mass transfer zone could be observed, slowing the progress towards equilibrium when there is no longer any mass transfer. A larger removal percentage was shown in the column because a greater bed height resulted in a greater amount of THI being eliminated. These results align with the conclusions presented in previous studies (González-López et al., 2020; Topare and Bokil, 2021).

Table 7. Breakthrough curve parameters of the studied flow rates

Flowrate (mL/min)	t_{total} (min)	V_{eff} (mL)	q_{total} (mg)	m_{total} (mg)	% Removal
1	116	116	0.41	1.74	23.56
4	30	120	0.036	1.8	2

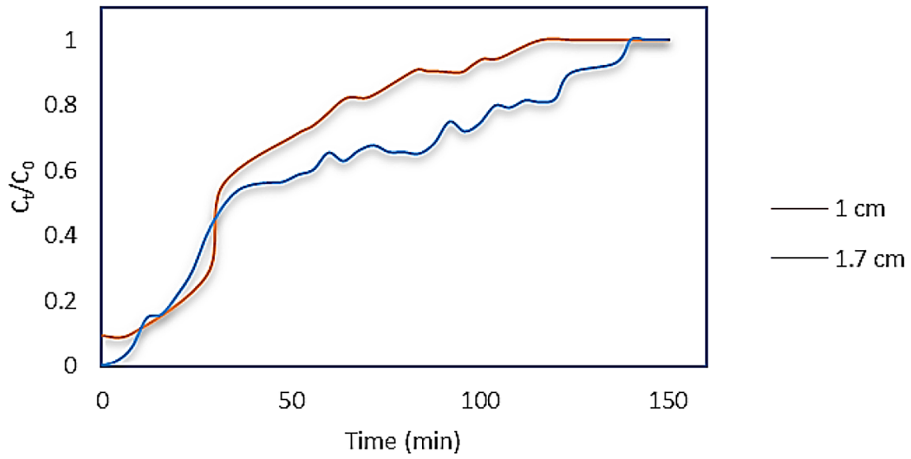

Figure 8. Curves obtained at various bed-heights

Table 8. Breakthrough curve parameters of the studied bed height

Bed height (cm)	t_{total} (min)	V_{eff} (mL)	q_{total} (mg)	m_{total} (mg)	% Removal
1	116	116	0.41	1.74	23.56
1.7	140	140	0.59	2.1	28.10

Initial concentration effect

In the column investigation, the THI adsorption is significantly impacted by the starting concentration. The THI concentration ranged between 5.5 mg/L and 15 mg/L, the remaining operational parameters remained steady, with 1 cm in bed-height and 1 mL·min^{-1} as flow rate. Figure 9 illustrates the curves depicting the impact of initial THI concentration. Breakthrough curves were associated with higher initial concentrations, which became slower as the initial concentration decreased. Table 9 indicates that as the initial THI increases, the effluent volume decreases from 150 mL to 116 mL. A shorter period was required to reach equilibrium for the elimination of THI at higher concentrations. From breakthrough curve 7 and Table 9, we conclude that the active sites on the adsorbent surface slowly filled at lower initial concentrations. The pores on the adsorbent rapidly filled at higher initial concentrations because at higher concentrations, large amounts of THI molecules were present. A low exhaustion time was achieved at greater concentrations because the adsorbent pores were filled with THI molecules over time.

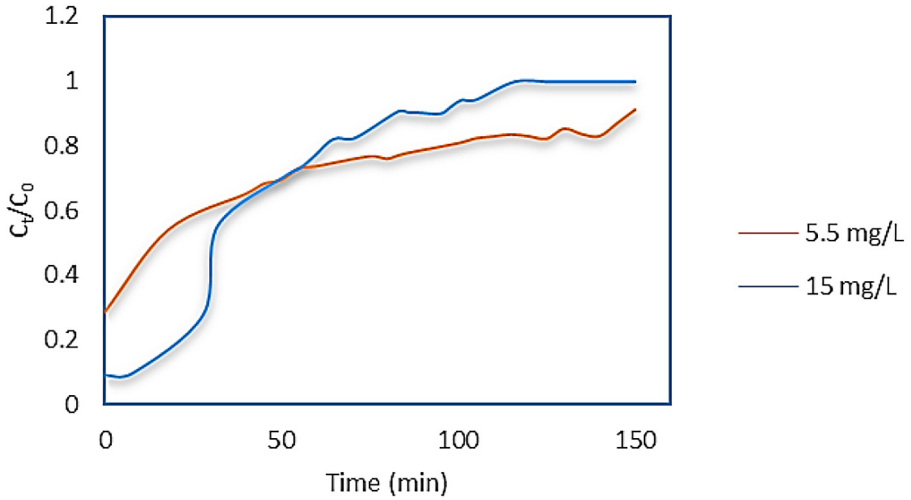

Figure 9. Breakthrough curves at different initial THI concentrations

Table 9. Breakthrough curve parameters of the studied bed high

Initial THI concentration (mg/L)	t_{total} (min)	V_{eff} (mL)	q_{total} (mg)	m_{total} (mg)	% Removal
5.5	150	150	0.43	0.83	51.81
15	116	116	0.41	1.74	23.56

CONCLUSION

Olive stone residues can be converted into activated carbons with specific textural properties. The resulting biomaterial exhibits exceptional characteristics, making it suitable for use in fixed-bed columns to remove micropollutants from water. Using OACPA, the maximum adsorption rate for THI reached 51.81%. These findings highlight the potential application of these materials in wastewater treatment processes.

Acknowledgements

I would like to express my gratitude to all the project teams at Umeå University and in South Africa for their expertise, assistance with the manuscript, and contributions to every aspect of our work.

REFERENCES

1. Al-Ghouti, M.A., Sweleh, A.O., 2019. Optimizing textile dye removal by activated carbon prepared from olive stones. Environmental Technology & Innovation 16, 100488. https://doi.org/10.1016/j.eti.2019.100488
2. Alslaibi, T.M., Abustan, I., Ahmad, M.A., Foul, A.A., 2013. Cadmium removal from aqueous solution using microwaved olive stone activated carbon. Journal of Environmental Chemical Engineering 1, 589–599. https://doi.org/10.1016/j.jece.2013.06.028
3. Álvarez-Torrellas, S., Rodríguez, A., Ovejero, G., García, J., 2016. Comparative adsorption performance of ibuprofen and tetracycline from aqueous solution by carbonaceous materials. Chemical Engineering Journal 283, 936–947. https://doi.org/10.1016/j.cej.2015.08.023
4. Asfaram, A., Ghaedi, M., Agarwal, S., Tyagi, I., Gupta, V.K., 2015. Removal of basic dye Auramine-O by ZnS:Cu nanoparticles loaded on activated carbon: optimization of parameters using response surface methodology with central composite design. RSC Advances 5, 18438–18450. https://doi.org/10.1039/C4RA15637D
5. Azmi, N.Bt., Bashir, M.J.K., Sethupathi, S., Wei, L.J., Aun, N.C., 2015. Stabilized landfill leachate treatment by sugarcane bagasse derived activated carbon for removal of color, COD and NH3-N – Optimization of preparation conditions by RSM. Journal of Environmental Chemical Engineering 3, 1287–1294. https://doi.org/10.1016/j.jece.2014.12.002
6. Azoulay, K., Bencheikh, I., Moufti, A., Dahchour, A., Mabrouki, J., El Hajjaji, S., 2020. Comparative study between static and dynamic adsorption efficiency of dyes by the mixture of palm waste using the central composite design. Chemical Data Collections 27, 100385. https://doi.org/10.1016/j.cdc.2020.100385
7. Baccar, R., Bouzid, J., Feki, M., Montiel, A., 2009. Preparation of activated carbon from Tunisian olive-waste cakes and its application for adsorption of heavy metal ions. Journal of Hazardous Materials 162, 1522–1529. https://doi.org/10.1016/j.jhazmat.2008.06.041
8. Baccar, R., Sarrà, M., Bouzid, J., Feki, M., Blánquez, P., 2012. Removal of pharmaceutical compounds by activated carbon prepared from agricultural by-product. Chemical Engineering Journal 211–212, 310–317. https://doi.org/10.1016/j.cej.2012.09.099
9. Balogoun, C.K., Bawa, M.L., Osseni, S., Aina, M., 2015. Préparation des charbons actifs par voie chimique à l'acide phosphorique à base de coque de noix de coco. International Journal of Biological and Chemical Sciences 9, 563–580. https://doi.org/10.4314/ijbcs.v9i1
10. Baş, D., Boyacı, İ.H., 2007. Modeling and optimization I: Usability of response surface methodology. Journal of Food Engineering 78, 836–845. https://doi.org/10.1016/j.jfoodeng.2005.11.024
11. Benaddi, H., Legras, D., Rouzaud, J.N., Beguin, F., 1998. Influence of the atmosphere in the chemical activation of wood by phosphoric acid. Carbon 36, 306–309. https://doi.org/10.1016/S0008-6223(98)80123-1
12. Bencheikh, I., Azoulay, K., Mabrouki, J., El Hajjaji, S., Moufti, A., Labjar, N., 2021. The use and the performance of chemically treated artichoke leaves for textile industrial effluents treatment. Chemical Data Collections 31, 100597. https://doi.org/10.1016/j.cdc.2020.100597
13. Benzekri, M.B., Benderdouche, N., Bestani, B., Douara, N., Duclaux, L., 2018. Valorization of olive stones into a granular activated carbon for the

removal of Methylene blue in batch and fixed bed modes. Journal of Materials and Environmental Science 9, 272.

14. Bestani, B., Benderdouche, N., Benstaali, B., Belhakem, M., Addou, A., 2008. Methylene blue and iodine adsorption onto an activated desert plant. Bioresource Technology 99, 8441–8444. https://doi.org/10.1016/j.biortech.2008.02.053
15. Bhattacharya, S., 2021. Central Composite Design for Response Surface Methodology and Its Application in Pharmacy. 1–19. https://doi.org/10.5772/intechopen.95835
16. Bouiti, K., Al-sharabi, H.A., Bouhlal, F., Abidi, B., Labjar, N., Bensemlali, M., Hajjaji, S.E., 2024. Response surface methodology for optimizing corrosion inhibition: investigating the synergistic effect of Eriobotrya japonica extract and potassium iodide. Euro-Mediterr J Environ Integr. https://doi.org/10.1007/s41207-023-00457-0
17. Busch, W., Schmidt, S., Kühne, R., Schulze, T., Krauss, M., Altenburger, R., 2016. Micropollutants in European rivers: A mode of action survey to support the development of effect-based tools for water monitoring. Environmental Toxicology and Chemistry 35, 1887–1899. https://doi.org/10.1002/etc.3460
18. Carvalho, I.T., Santos, L., 2016. Antibiotics in the aquatic environments: A review of the European scenario. Environment International 94, 736–757. https://doi.org/10.1016/j.envint.2016.06.025
19. Chakraborty, P., Show, S., Banerjee, S., Halder, G., 2018. Mechanistic insight into sorptive elimination of ibuprofen employing bi-directional activated biochar from sugarcane bagasse: Performance evaluation and cost estimation. Journal of Environmental Chemical Engineering 6, 5287–5300. https://doi.org/10.1016/j.jece.2018.08.017
20. Corral-Bobadilla, M., Lostado-Lorza, R., Somovilla-Gómez, F., Escribano-García, R., 2021. Effective use of activated carbon from olive stone waste in the biosorption removal of Fe(III) ions from aqueous solutions. Journal of Cleaner Production 294, 126332. https://doi.org/10.1016/j.jclepro.2021.126332
21. Cruz-Olivares, J., Pérez-Alonso, C., Barrera-Díaz, C., Ureña-Nuñez, F., Chaparro-Mercado, M.C., Bilyeu, B., 2013. Modeling of lead (II) biosorption by residue of allspice in a fixed-bed column. Chemical Engineering Journal 228, 21–27.
22. Das, S., Mishra, S., 2017. Box-Behnken statistical design to optimize preparation of activated carbon from Limonia acidissima shell with desirability approach. Journal of Environmental Chemical Engineering 5, 588–600. https://doi.org/10.1016/j.jece.2016.12.034
23. Deblonde, T., Cossu-Leguille, C., Hartemann, P., 2011. Emerging pollutants in wastewater: A review of the literature. International Journal of Hygiene and Environmental Health, The second European PhD students workshop: Water and health ? Cannes 2010 214, 442–448. https://doi.org/10.1016/j.ijheh.2011.08.002
24. Dehkhoda, A.M., Ellis, N., Gyenge, E., 2014. Electrosorption on activated biochar: effect of thermochemical activation treatment on the electric double layer capacitance. J Appl Electrochem 44, 141–157. https://doi.org/10.1007/s10800-013-0616-4
25. Delgado, N., Marino, D., Capparelli, A., Casas-Zapata, J.C., Navarro, A., 2022. Pharmaceutical compound removal using down-flow fixed bed filters with powder activated carbon: A novel configuration. Journal of Environmental Chemical Engineering 10, 107706. https://doi.org/10.1016/j.jece.2022.107706
26. DemiRoğlu, S., Erdoğan, F., Akin, E., Karavana, H.A., Özgür, M., 2017. Natural Fiber Reinforced Polyurethane Rigid Foam 13.
27. Di Leo, G., Sardanelli, F., 2020. Statistical significance: p value, 0.05 threshold, and applications to radiomics—reasons for a conservative approach. European Radiology Experimental 4, 18. https://doi.org/10.1186/s41747-020-0145-y
28. dos Reis, G.S., Wilhelm, M., Silva, T.C. de A., Rezwan, K., Sampaio, C.H., Lima, E.C., de Souza, S.M.A.G.U., 2016. The use of design of experiments for the evaluation of the production of surface rich activated carbon from sewage sludge via microwave and conventional pyrolysis. Applied Thermal Engineering 93, 590–597. https://doi.org/10.1016/j.applthermaleng.2015.09.035
29. Durán-Valle, C., Gómez-Corzo, M., Pastor-Villegas, J., Gómez-Serrano, V., 2005. Study of cherry stones as raw material in preparation of carbonaceous adsorbents. Journal of Analytical and Applied Pyrolysis - J ANAL APPL PYROL 73, 59–67. https://doi.org/10.1016/j.jaap.2004.10.004
30. Elabdouni, A., Haboubi, K., Merimi, I., El Youbi, M.S.M., 2020. Olive mill wastewater (OMW) production in the province of Al-Hoceima (Morocco) and their physico-chemical characterization by mill types. Materials Today: Proceedings, The Third International Conference on Materials and Environmental Science 27, 3145–3150. https://doi.org/10.1016/j.matpr.2020.03.806
31. Fallah, N., Taghizadeh, M., 2020. Continuous fixed-bed adsorption of Mo(VI) from aqueous solutions by Mo(VI)-IIP: Breakthrough curves analysis and mathematical modeling. Journal of Environmental Chemical Engineering 8, 104079. https://doi.org/10.1016/j.jece.2020.104079
32. Freitas, J.V., Nogueira, F.G.E., Farinas, C.S., 2019. Coconut shell activated carbon as an alternative adsorbent of inhibitors from lignocellulosic biomass pretreatment. Industrial Crops and

Products 137, 16–23. https://doi.org/10.1016/j.indcrop.2019.05.018

33. García-Mateos, F.J., Ruiz-Rosas, R., Marqués, M.D., Cotoruelo, L.M., Rodríguez-Mirasol, J., Cordero, T., 2015. Removal of paracetamol on biomass-derived activated carbon: Modeling the fixed bed breakthrough curves using batch adsorption experiments. Chemical Engineering Journal 279, 18–30. https://doi.org/10.1016/j.cej.2015.04.144
34. Gomez-Serrano, V., Pastor-Villegas, J., Duran-Valle, C.J., Valenzuela-Calahorro, C., 1996. Heat treatment of rockrose char in air. Effect on surface chemistry and porous texture. Carbon 34, 533–538. https://doi.org/10.1016/0008-6223(96)00001-2
35. González-López, M.E., Pérez-Fonseca, A.A., Arellano, M., Gómez, C., Robledo-Ortíz, J.R., 2020. Fixed-bed adsorption of Cr(VI) onto chitosan supported on highly porous composites. Environmental Technology & Innovation 19, 100824. https://doi.org/10.1016/j.eti.2020.100824
36. Gueye, M., Richardson, Y., Kafack, F.T., Blin, J., 2014. High efficiency activated carbons from African biomass residues for the removal of chromium(VI) from wastewater. Journal of Environmental Chemical Engineering 2, 273–281. https://doi.org/10.1016/j.jece.2013.12.014
37. Hameed, B.H., Tan, I.A.W., Ahmad, A.L., 2008. Optimization of basic dye removal by oil palm fibre-based activated carbon using response surface methodology. Journal of Hazardous Materials 158, 324–332. https://doi.org/10.1016/j.jhazmat.2008.01.088
38. Hazzaa, R., Hussein, M., 2015. Adsorption of cationic dye from aqueous solution onto activated carbon prepared from olive stones. Environmental Technology & Innovation 4, 36–51. https://doi.org/10.1016/j.eti.2015.04.002
39. Heidarinejad, Z., Dehghani, M.H., Heidari, M., Javedan, G., Ali, I., Sillanpää, M., 2020a. Methods for preparation and activation of activated carbon: a review. Environ Chem Lett 18, 393–415. https://doi.org/10.1007/s10311-019-00955-0
40. Heidarinejad, Z., Dehghani, M.H., Heidari, M., Javedan, G., Ali, I., Sillanpää, M., 2020b. Methods for preparation and activation of activated carbon: a review. Environ Chem Lett 18, 393–415. https://doi.org/10.1007/s10311-019-00955-0
41. Hu, J., Shen, D., Wu, S., Zhang, H., Xiao, R., 2014. Effect of temperature on structure evolution in char from hydrothermal degradation of lignin. Journal of Analytical and Applied Pyrolysis 106, 118–124. https://doi.org/10.1016/j.jaap.2014.01.008
42. Iheanacho, O.C., Nwabanne, J.T., Obi, C.C., Onu, C.E., 2021. Packed bed column adsorption of phenol onto corn cob activated carbon: linear and non-linear kinetics modeling. South African Journal of Chemical Engineering 36, 80–93. https://doi.org/10.1016/j.sajce.2021.02.003
43. Ismail, I.S., Rashidi, N.A., Yusup, S., 2022. Production and characterization of bamboo-based activated carbon through single-step H3PO4 activation for CO2 capture. Environmental Science and Pollution Research 29, 12434–12440. https://doi.org/10.1007/s11356-021-15030-x
44. Itodo, A.U., Abdulrahman, F.W., Hassan, L.G., Maigandi, S.A., Itodo, H.U., 2010. Application of methylene blue and iodine adsorption in the measurement of specific surface area by four acid and salt treated activated carbons. New York science journal 3, 25–33.
45. Jamil, F., Al-Muhtaseb, A.H., Naushad, M., Baawain, M., Al-Mamun, A., Saxena, S.K., Viswanadham, N., 2020. Evaluation of synthesized green carbon catalyst from waste date pits for tertiary butylation of phenol. Arabian Journal of Chemistry 13, 298–307. https://doi.org/10.1016/j.arabjc.2017.04.009
46. Jawad, A.H., Ishak, M.M., Farhan, A.M., Ismail, K., 2017. Response surface methodology approach for optimization of color removal and COD reduction of methylene blue using microwave-induced NaOH activated carbon from biomass waste. Water Treat 62, 208–220.
47. Jiang, G., Qiao, J., Hong, F., 2012. Application of phosphoric acid and phytic acid-doped bacterial cellulose as novel proton-conducting membranes to PEMFC. International Journal of Hydrogen Energy 37, 9182–9192. https://doi.org/10.1016/j.ijhydene.2012.02.195
48. Jodeh, S., Abdelwahab, F., Jaradat, N., Warad, I., Jodeh, W., 2016. Adsorption of diclofenac from aqueous solution using Cyclamen persicum tubers based activated carbon (CTAC). Journal of the Association of Arab Universities for Basic and Applied Sciences 20, 32–38. https://doi.org/10.1016/j.jaubas.2014.11.002
49. Kavianinia, I., Plieger, P.G., Kandile, N.G., Harding, D.R.K., 2012. Fixed-bed column studies on a modified chitosan hydrogel for detoxification of aqueous solutions from copper (II). Carbohydrate Polymers 90, 875–886. https://doi.org/10.1016/j.carbpol.2012.06.014
50. Kaya, N., Atagur, M., Akyuz, O., Seki, Y., Sarikanat, M., Sutcu, M., Seydibeyoglu, M.O., Sever, K., 2018. Fabrication and characterization of olive pomace filled PP composites. Composites Part B: Engineering 150, 277–283. https://doi.org/10.1016/j.compositesb.2017.08.017
51. Li, K., Zhang, P., Ge, L., Ren, H., Yu, C., Chen, X., Zhao, Y., 2014. Concentration-dependent photodegradation kinetics and hydroxyl-radical oxidation of phenicol antibiotics. Chemosphere 111, 278–282. https://doi.org/10.1016/j.chemosphere.2014.04.052

52. Li, S., Han, K., Li, J., Li, M., Lu, C., 2017. Preparation and characterization of super activated carbon produced from gulfweed by KOH activation. Microporous and Mesoporous Materials 243, 291–300. https://doi.org/10.1016/j.micromeso.2017.02.052
53. Luo, Y., Guo, W., Ngo, H.H., Nghiem, L.D., Hai, F.I., Zhang, J., Liang, S., Wang, X.C., 2014. A review on the occurrence of micropollutants in the aquatic environment and their fate and removal during wastewater treatment. Science of The Total Environment 473–474, 619–641. https://doi.org/10.1016/j.scitotenv.2013.12.065
54. Mailler, R., Gasperi, J., Patureau, D., Vulliet, E., Delgenes, N., Danel, A., Deshayes, S., Eudes, V., Guerin, S., Moilleron, R., Chebbo, G., Rocher, V., 2017. Fate of emerging and priority micropollutants during the sewage sludge treatment: Case study of Paris conurbation. Part 1: Contamination of the different types of sewage sludge. Waste Management 59, 379–393. https://doi.org/10.1016/j.wasman.2016.11.010
55. Maita, K., Kuwahara, M., Kosaka, T., Inui, K., Sugimoto, K., Takeuchi, Y., Hatakenaka, N., Harada, T., Yasuhara, K., Mitsumori, K., 1999. Testicular Toxicity of Thiamphenicol in Sprague-Dawley Rats. Journal of Toxicologic Pathology 12, 27–27. https://doi.org/10.1293/tox.12.27
56. Mansouri, H., Carmona, R.J., Gomis-Berenguer, A., Souissi-Najar, S., Ouederni, A., Ania, C.O., 2015. Competitive adsorption of ibuprofen and amoxicillin mixtures from aqueous solution on activated carbons. Journal of Colloid and Interface Science, Liquid Films, Interfaces and Colloidal Dispersions 449, 252–260. https://doi.org/10.1016/j.jcis.2014.12.020
57. Miguet, M., Goetz, V., Plantard, G., Jaeger, Y., 2016. Sustainable Thermal Regeneration of Spent Activated Carbons by Solar Energy: Application to Water Treatment. Ind. Eng. Chem. Res. 55, 7003–7011. https://doi.org/10.1021/acs.iecr.6b01260
58. Mustafa, I., Fathurrahmi, Suriarah, Farida, M., Ahmad, K., 2022. Palm shell-derived activated carbon adsorbent is better than that of coconut shell: comparative studies of cod adsorption from palm oil mill effluent. Rasayan Journal of Chemistry 15, 738–744. https://doi.org/10.31788/RJC.2022.1526804
59. Patel, P., Gupta, S., Mondal, P., 2022. Modeling of continuous adsorption of greywater pollutants onto sawdust activated carbon bed integrated with sand column. Journal of Environmental Chemical Engineering 10, 107155. https://doi.org/10.1016/j.jece.2022.107155
60. Putra, E.K., Pranowo, R., Sunarso, J., Indraswati, N., Ismadji, S., 2009. Performance of activated carbon and bentonite for adsorption of amoxicillin from wastewater: Mechanisms, isotherms and kinetics. Water Research 43, 2419–2430. https://doi.org/10.1016/j.watres.2009.02.039
61. Rosene, M.R., Ozcan, M., Manes, M., 1976. Application of the Polanyi adsorption potential theory to adsorption from solution on activated carbon. 8. Ideal, nonideal, and competitive adsorption of some solids from water solution. J. Phys. Chem. 80, 2586–2589. https://doi.org/10.1021/j100564a011
62. Sabio, E., Zamora, F., Gañan, J., González-García, C.M., González, J.F., 2006. Adsorption of p-nitrophenol on activated carbon fixed-bed. Water Research 40, 3053–3060. https://doi.org/10.1016/j.watres.2006.06.018
63. Samghouli, N., Bencheikh, I., Azoulay, K., Abahdou, F.-Z., Mabrouki, J., El Hajjaji, S., 2022. Study of Piroxicam Removal from Wastewater by Artichoke Waste Using NemrodW® Software: Statistical Analysis. 29–42. https://doi.org/10.1007/978-3-030-90083-0_3
64. Senthilkumar, T., Chattopadhyay, S.K., Miranda, L.R., 2017. Optimization of activated carbon preparation from pomegranate peel (*Punica granatum* Peel) using RSM. Chemical Engineering Communications 204, 238–248. https://doi.org/10.1080/00986445.2016.1262358
65. Seydibeyoğlu, M.Ö., Demiroglu, S., Erdoğan, F., Akın, E., Ayvalık, A., Karavana, H.A., 2017. Natural Fiber Reinforced Polyurethane Rigid Foam [WWW Document]. undefined. URL /paper/NATURAL-FIBER-REINFORCED-POLYURETHANE-RIGID-FOAM-Seydibeyo%C4%9Flu-Demiroglu/dd0eff97a680d2c8b0c57ee08f428f481617fbcc (accessed 10.2.20).
66. Sim, W.-J., Lee, J.-W., Lee, E.-S., Shin, S.-K., Hwang, S.-R., Oh, J.-E., 2011. Occurrence and distribution of pharmaceuticals in wastewater from households, livestock farms, hospitals and pharmaceutical manufactures. Chemosphere 82, 179–186. https://doi.org/10.1016/j.chemosphere.2010.10.026
67. Song, J., Zou, W., Bian, Y., Su, F., Han, R., 2011. Adsorption characteristics of methylene blue by peanut husk in batch and column modes. Desalination 265, 119–125. https://doi.org/10.1016/j.desal.2010.07.041
68. Sotelo, J.L., Ovejero, G., Rodríguez, A., Álvarez, S., Galán, J., García, J., 2014. Competitive adsorption studies of caffeine and diclofenac aqueous solutions by activated carbon. Chemical Engineering Journal 240, 443–453. https://doi.org/10.1016/j.cej.2013.11.094
69. Sotelo, J.L., Rodríguez, A., Álvarez, S., García, J., 2012a. Removal of caffeine and diclofenac on activated carbon in fixed bed column. Chemical Engineering Research and Design 90, 967–974. https://doi.org/10.1016/j.cherd.2011.10.012
70. Sotelo, J.L., Rodríguez, A., Álvarez, S., García, J., 2012b. Removal of caffeine and diclofenac on activated carbon in fixed bed column. Chemical

Engineering Research and Design 90, 967–974. https://doi.org/10.1016/j.cherd.2011.10.012

71. Suhas, Gupta, V.K., Carrott, P.J.M., Singh, R., Chaudhary, M., Kushwaha, S., 2016. Cellulose: A review as natural, modified and activated carbon adsorbent. Bioresource Technology 216, 1066–1076. https://doi.org/10.1016/j.biortech.2016.05.106
72. Sun, Y., Yue, Q., Gao, B., Huang, L., Xu, X., Li, Q., 2012. Comparative study on characterization and adsorption properties of activated carbons with H3PO4 and H4P2O7 activation employing Cyperus alternifolius as precursor. Chemical Engineering Journal 181–182, 790–797. https://doi.org/10.1016/j.cej.2011.11.098
73. Tarley, C.R.T., Silveira, G., dos Santos, W.N.L., Matos, G.D., da Silva, E.G.P., Bezerra, M.A., Miró, M., Ferreira, S.L.C., 2009. Chemometric tools in electroanalytical chemistry: Methods for optimization based on factorial design and response surface methodology. Microchemical Journal, Polar Chemistry 92, 58–67. https://doi.org/10.1016/j.microc.2009.02.002
74. Topare, N.S., Bokil, S.A., 2021. Adsorption of textile industry effluent in a fixed bed column using activated carbon prepared from agro-waste materials. Materials Today: Proceedings, 1st International Conference on Energy, Material Sciences and Mechanical Engineering 43, 530–534. https://doi.org/10.1016/j.matpr.2020.12.029
75. Xu, F., Yu, J., Tesso, T., Dowell, F., Wang, D., 2013. Qualitative and quantitative analysis of lignocellulosic biomass using infrared techniques: A mini-review. Applied Energy 104, 801–809. https://doi.org/10.1016/j.apenergy.2012.12.019